www.czasopisma.pan.pl PAN www.journals.pan.pl
Opto-Electronics Review 26 (2018) 57–62

Contents lists available at ScienceDirect

Opto-Electronics Review

journal homepage: http://www.journals.elsevier.com/opto-electronics review

Optimization of microstructured fibers with germanium-doped core for broad normal dispersion range

J. Biedrzycki, K. Tarnowski*, W. Urbańczyk*

Department of Optics and Photonics, Faculty of Fundamental Problems of Technology, Wroclaw University of Science and Technology, Wybrzeże Wyspianskiego 27, 50-370 Wroclaw, Poland

ARTICLE INFO

Article history:
Received 16 May 2017
Received in revised form
21 November 2017
Accepted 22 January 2018
Available online 7 February 2018

Keywords:
Nonlinear optics
Fibers
Supercontinuum generation
Silica
Dispersion
Microstructured fibers

ABSTRACT

We have numerically studied different designs of technologically feasible microstructured fibers with a germanium-doped core in order to obtain normal dispersion reaching possibly far in the mid infrared. Hexagonal, Kagome and the combination of both geometries were numerically examined with respect to different constructional parameters like pitch distance, filling factor of air holes, number of layers surrounding the core, and level of germanium doping in the core. Our analysis showed that the broadest range of normal dispersion reaching 2.81 μm, while keeping an effective mode area smaller than 30 μm^2, was achieved for a hexagonal lattice and a 40 mol% GeO_2 doped core. The proposed fibers designs can be used in generation of a normal dispersion supercontinuum reaching the mid-IR region.

1. Introduction

Since the first demonstration of supercontinuum (SC) in microstructured fibers [1], these new light sources found numerous applications in different fields, including optical coherence tomography [2], confocal microscopy [3], and metrology [4]. Initially, the large spectral broadening was obtained by pumping the microstructured fiber slightly above the zero dispersion wavelength, i.e. in the anomalous chromatic dispersion range. In this way, the ultra-broad spectrum can be obtained, however, composed of many pulses in time domain and having non-uniform power spectral density [5].

Recently, it has been demonstrated that pumping an all-normal dispersion (ANDi) fiber causes generation of spectrally broad SC characterized by a flat time-frequency profile, high stability and coherence [6,7]. For effective generation of ANDi SC, it is required that the pump wavelength matches the local maximum of a dispersion curve, which results in SC characterized by flat and octave spanning spectrum with the high degree of pulse-to-pulse coherence [8]. First ANDi SC has been obtained in silica microstructured fibers pumped at 1050 nm and 650 nm. It covered the spectral range from 0.5 μm to 1.5 μm [6]. Since that time many simulations and experimental efforts have been reported in literature to shift the all normal dispersion SC towards the mid-infrared. Most of them are based on fibers made of exotic glasses, like silica heavily doped by GeO_2 (60 to 100 mol%) [9], lead-silicate glass [10], borosilicate glass with flint glass inclusions [8,11,12], chalcogenide glass [13,14], tellurite glass [15] and hybrid fibers combining sections with anomalous and normal dispersion [16].

As the transparency window of silica glass reaches 2.8 μm [17], some efforts have been also undertaken to obtain mid-infrared shifted ANDi SC in silica fibers, which are compatible with telecommunication technology. The silica ANDi fibers can be easily spliced with standard telecommunication fibers thanks to close softening temperatures and processed employing equipment typically used in telecommunication. It has been demonstrated both numerically [18] and experimentally [19] that it is possible to obtain a flattened normal dispersion in the spectral range up to 2.3 μm in a specially designed microstructured fiber with GeO_2 doped inclusion surrounded by small holes. The process of SC generation was studied experimentally in this fiber using a pulse laser operating at 1.56 μm. with a pulse duration of 23 fs. The experimental results proved that the ANDi SC generated in this fiber spreads from 1.2 μm to 2.2 μm. In the most recent paper the PolAND SC (polarized all-normal dispersion supercontinuum) was demonstrated from 1.0 μm to 2.5 μm [20].

Another approach was investigated numerically in Ref. [21]. By tailoring the structural parameters of an air–silica microstructured fiber, a flattened normal dispersion reaching 3 μm has been

* Correspondingauthors.
E-mail addresses: karol.tarnowski@pwr.edu.pl (K. Tarnowski), waclaw.urbanczyk@pwr.edu.pl (W. Urbańczyk).

https://doi.org/10.1016/j.opelre.2018.01.004
1230-3402/

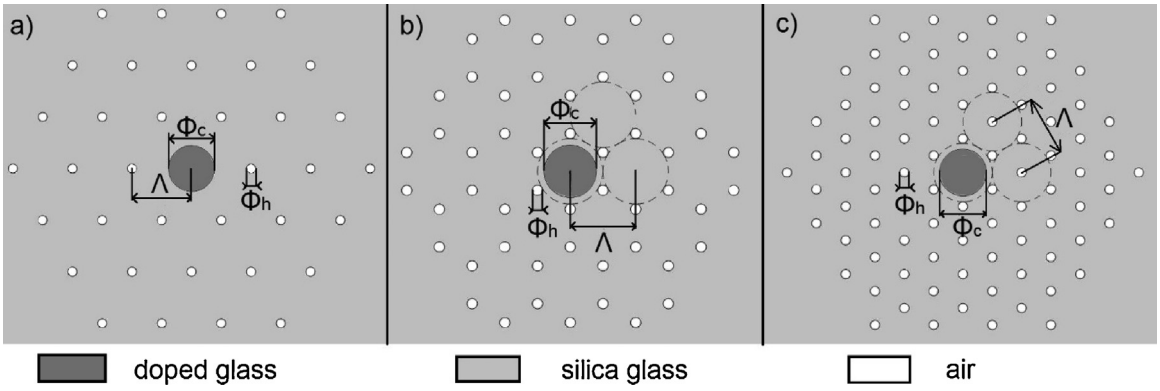

Fig. 1. Cross-sections of the fibers with germanium doped core surrounded by microstructured region of hexagonal symmetry (a), Kagome symmetry (b), and combination of both (c), Φ_c indicates the diameter of germanium doped core, Φ_h – diameter of air holes, Λ – lattice pitch.

obtained, thus allowing for ANDi SC generation in the spectral range of 1 μm–2.2 μm by pumping the fiber at 1.55 μm.

In this paper we study the possibility of further increase in the normal dispersion range towards the silica transmission cutoff in the mid-infrared [17] in the microstructured fiber first proposed in Ref. [18], having a germanium doped core surrounded by one layer of holes. We demonstrated by numerical simulations that by tuning geometrical parameters of the fiber, such as GeO_2 concentration in the core, diameter of the core, pitch distance, size of air holes and the number of holes' layers, it is possible to extend the normal dispersion range up to 2.81 μm. This makes a significant progress with respect to the fiber design reported in Ref. [18] with 18 mol% of GeO_2 in the core and one layer of holes surrounding the core, in which all normal dispersion range reaches 2.3 μm. Therefore, the proposed fiber design gives a good prospect to fully cover a long wavelength part of the transparency window of silica fibers with coherent SC generated in the normal dispersion regime.

2. Fiber structure and computation method

Considered fiber structures are shown in Fig. 1. A germanium doped core of the diameter Φ_c is surrounded by up to three layers of air holes of the diameter Φ_h. The number of holes' layers is denoted by N. We have numerically analyzed only such fiber structures which are feasible in stack and draw technology. In order to achieve those feasibility specific relations between the holes' diameters, the lattice constant Λ and the core diameter must be met. Therefore, it is assumed in all the considered fiber geometries that the rod/capillaries used to stack the microstructured region are of the same external diameter. Three technologically feasible microstructure symmetries were considered, respectively hexagonal, Kagome and the combination of both (Fig. 1). An important advantage of the Kagome geometry is that the first ring of air holes is located closest to the germanium doped region.

Numerical simulations were conducted using the finite element method implemented in Comsol Multiphysics Wave Optics Module. First, we calculated the spectral dependence of the effective mode index and field distributions, taking into account Sellmeier's equations for germanium doped and pure silica glass [22,23]. Triangular mesh of finite elements defining the fiber geometry and the second order shape function describing computed electric field were used. The maximum size of finite elements were equal, respectively to 0.05 μm for the core and holes, 0.2 μm for the cladding and 0.5 μm for the perfectly matched layer (PML). Basing on the convergence criteria, we estimated a numerical error in computing the real part of the mode effective index at 10^{-6}. Similarly as in Ref. [16], the parameters essential in PML implementation were selected basing on the calculation of the effective mode area (A_{eff}). For the cladding diameter of 125 μm, the thickness of PML of 3 μm and the PML scaling factor of 3, the differences in computed A_{eff} between the models with impedance boundary conditions (IBC) and perfect electric conductor on the outside border of PML were lower than 1% for wavelengths of 0.5 μm and 3 μm, which are the limits of the examined spectral range. All the calculations of the effective index were conducted using IBC outside PML.

The field distribution was used to evaluate an effective nonlinear refractive index n_2 for the supported mode. The effective nonlinear index can be calculated as a weighted average of the nonlinear refractive index of constituent materials [24]. We disregarded the wavelength dependence of the nonlinear refractive index and approximated it for pure and GeO_2-doped silica glass according to the formula $n_2 = 2.507 + 0.505\Delta$ [10^{-20} m^2/W], where Δ is the relative index difference of doped and undoped glass at 1.5 μm [24].

Finally, the calculated real part of the effective index of the fundamental mode with the wavelength step of 10 nm was numerically differentiated to determine a chromatic dispersion. The imaginary part of the effective index was used to calculate a confinement loss. For fibers with microstructured cladding, the numerical simulations were limited only to the spectral range, at which $A_{eff} < 30\ \mu m^2$. Such condition assures that the fundamental core mode is not at cut-off, although in a long wavelength range, the nonlinearity will be limited and bend loss will be significant. Experimental results presented in Ref. [19] show that the generated supercontinuum reaches 2.2 μm whereas the effective area is 30 μm^2 at this wavelength. It confirms that for $A_{eff} < 30\ \mu m^2$ the efficient SC broadening can be obtained.

3. Simulation results

In the first step, we calculated the chromatic dispersion for the fiber without any microstructure for two levels of GeO_2 doping in the core, respectively equal to 40 mol% and 20 mol%. We chose 40 mol% as a maximal doping level because this is close to the highest concentration of GeO_2 reported for fabricated microstructured optical fibers [25]. For the two GeO_2 concentrations, a number of core diameters providing the first order mode cut-off in the range from 0.8 to 1.8 μm with the step of 0.2 μm were examined. According to the results displayed in Fig. 2, a greater doping level broadens the range of normal dispersion. Among examined step index fibers with the core doping of 40 mol%, the broadest range of normal dispersion (upto 2.75 μm) was obtained for the core diameter Φ_c = 2.5 μm [Fig. 2(a)], while for the core doping of 20 mol%, the broadest normal dispersion range (upto 2.20 μm) was achieved for Φ_c = 3 μm [Fig. 2(b)].

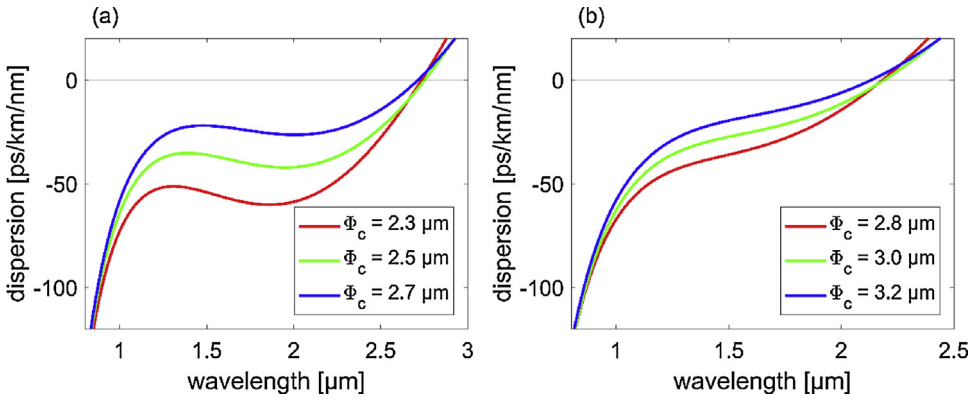

Fig. 2. Chromatic dispersion calculated for a step index fiber with 40 mol% (a) and 20 mol% (b) germanium doped core of different diameters Φ_c.

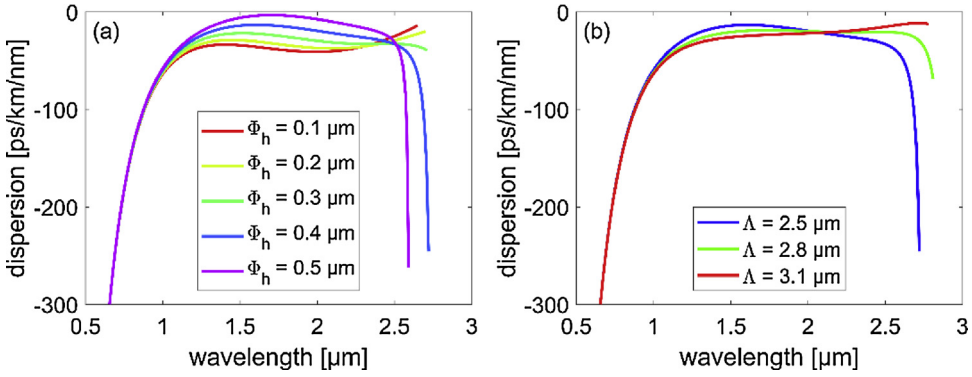

Fig. 3. First two steps of optimization procedure for the fiber with hexagonal lattice with the core doped with 40 mol% of GeO_2 and core diameter $\Phi_c = 2.5$ μm: finding an optimal holes diameter Φ_h for fixed lattice constant $\Lambda = \Phi_c$ (a) and finding optimal lattice constant Λ for fixed holes diameter $\Phi_h = 0.4$ μm (b).

Optimization of the cladding microstructure composed of three layers of holes was performed for the core dimeter assuring the largest normal dispersion rage, i.e. $\Phi_c = 2.5$ μm for 40 mol% and $\Phi_c = 3.0$ μm for 20 mol%. First, the lattice constant is fixed at $\Lambda = \Phi_c$ and the hole diameters (Φ_h) were varied until the normal dispersion range reached the maximum value. The procedure of scanning the hole diameters Φ_h with a step of 0.1 μm is illustrated in Fig. 3(a). For hexagonal lattice and doping of 40 mol%, the optimum value of the holes diameter was found to be $\Phi_h = 0.4$ μm. In the next step, for fixed $\Phi_h = 0.4$ μm, we scanned the lattice constant Λ to achieve the largest normal dispersion range. As illustrated in Fig. 3(b), for hexagonal symmetry, the lattice constant $\Lambda = 2.8$ μm yields the broadest normal dispersion. Finally, another step of optimization for the fixed lattice constant $\Lambda = 2.8$ μm was conducted in order to find the optimal value of holes diameter Φ_h. The scanning of Φ_h was done with a step of 0.05 μm. For hexagonal symmetry, 40 mol% doping and lattice constant $\Lambda = 2.8$ μm, the broadest normal dispersion range, reaching up to 2.81 μm, was achieved for $\Phi_h = 0.40$ μm.

For the dispersion profile presented in Fig. 3 we observed an unexpected behaviour in a long wavelength limit, namely a deep decrease to negative values. We verified that this is related to the mode cut-off and sudden increase in confinement loss. In Fig. 4 we present the calculated confinement loss corresponding to the dispersion profiles presented in Fig. 3.

Similar optimization approach was applied for the fibers with the core doped with 20 mol% of GeO_2. In this case, the optimal geometrical parameters assuring normal dispersion up to 2.25 μm are as follows: $\Phi_c = 3.0$ μm, $\Lambda = 3.2$ μm and $\Phi_h = 0.40$ μm. Moreover, to examine the impact of successive holes layers on the dispersion characteristics, we performed the simulations for only 1 and 2 layers of holes, while keeping the lattice constant and hole diameters fixed. The results displayed in Fig. 5 show that the introduction of the second and the third layer of holes broadens the normal dispersion range. Similar three-step optimization procedure was applied to examine the fibers with Kagome lattice and the combination of hexagonal and Kagome lattices.

Optimization performed for the fiber with Kagome lattice having 3 layers of holes showed the best results for the core doping of 40 mol% and $\Phi_c = 2.5$ μm, $\Lambda = 3.8$ μm, $\Phi_h = 0.25$ μm. Such combination of the fiber parameters assures normal dispersion reaching 2.70 μm, while keeping $A_{eff} \leq 30\ \mu m^2$. For the core doping of 20 mol%, normal dispersion reaching 2.11 μm for $A_{eff} \leq 30\ \mu m^2$ was obtained for the following set of parameters $\Phi_c = 3.0$ μm, $\Lambda = 4.0$ μm, and $\Phi_h = 0.25$ μm. The calculated dispersion curves for both doping levels and different numbers of holes layers $N = 1$, 2 and 3 are shown in Fig. 6.

Simulations of the fiber with combined hexagonal and Kagome lattice have shown the best results for the following set of parameters: $\Phi_c = 2.5$ μm, $\Lambda = 3.3$ μm, $\Phi_h = 0.25$ μm for 40 mol% of GeO_2 doping and $\Phi_c = 3.0$ μm, $\Lambda = 3.6$ μm, $\Phi_h = 0.20$ μm for 20 mol% of GeO_2 doping. Such fiber geometries assure the normal dispersion range for $A_{eff} \leq 30\ \mu m^2$ up to 2.72 μm and 2.13 μm, respectively for 40 mol% and 20 mol% of GeO_2 doping, as it is shown in Fig. 7.

Spectral dependences of the effective mode area A_{eff} up to the limiting value of 30 μm^2 for the fibers with optimal parameters are shown in Fig. 8. In Fig. 9 we present the calculated confinement loss for the optimized designs. The obtained results show that the fundamental modes are approaching cut-off in the considered spectral range. For the sake of completeness, Figure 10 presents the calculated nonlinear coefficient $\gamma = \frac{n_2 \omega}{c A_{eff}}$ for the optimized fiber designs.

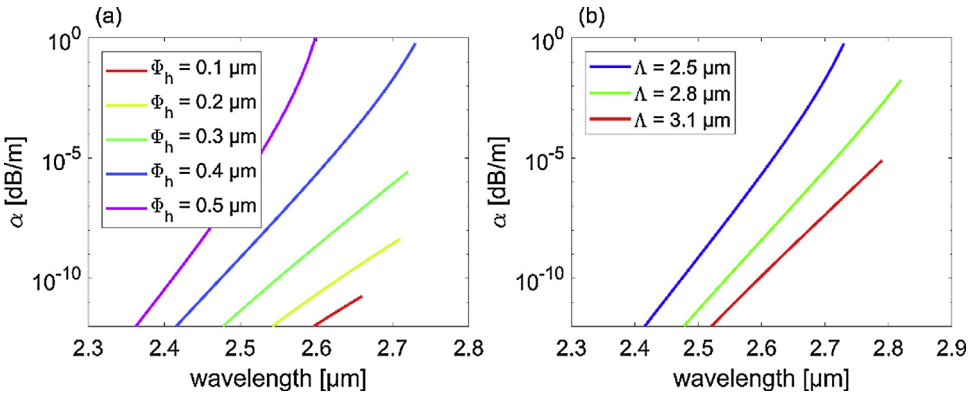

Fig. 4. Calculated confinement loss in the first two steps of the optimization procedure for the fiber with hexagonal lattice and core doped with 40 mol% of GeO_2, core diameter Φ_c = 2.5 μm: finding an optimal holes diameter Φ_h for fixed lattice constant $\Lambda = \Phi_c$ (a) and finding optimal lattice constant Λ for fixed holes diameter Φ_h = 0.4 μm (b).

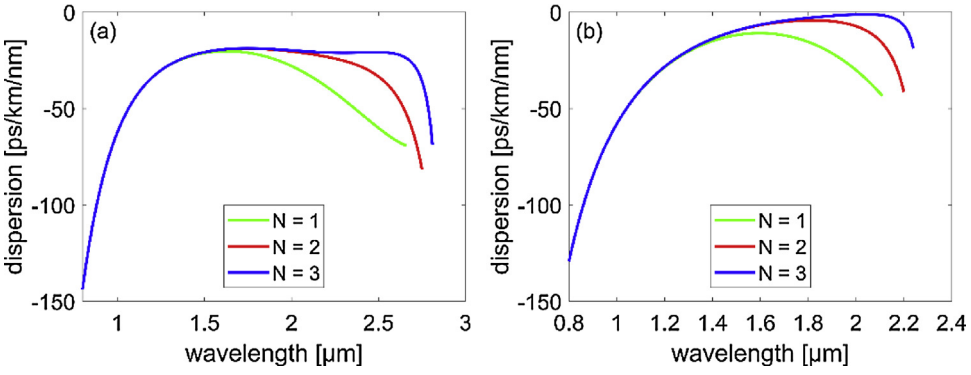

Fig. 5. Chromatic dispersion calculated for different numbers of holes layers (N) for the fiber with hexagonal lattice and 40 mol% of GeO_2 doping, Φ_c = 2.5 μm, Λ = 2.8 μm and Φ_h = 0.40 μm (a) and 20 mol% of GeO_2 doping, Φ_c = 3.0 μm, Λ = 3.2 μm and Φ_h = 0.40 μm (b).

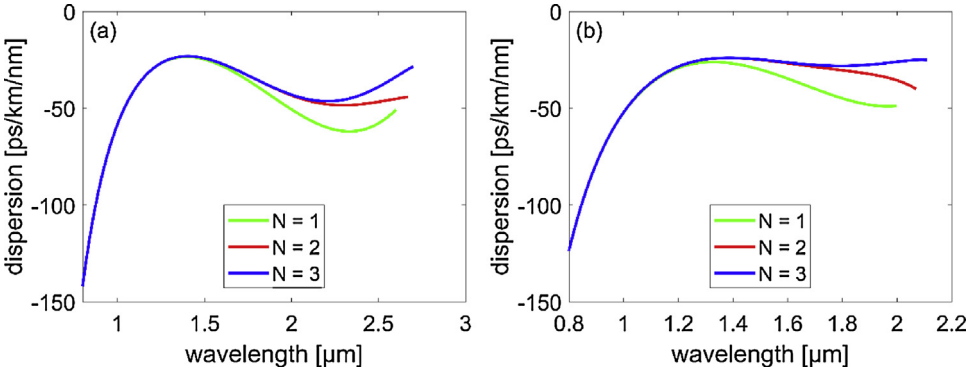

Fig. 6. Chromatic dispersion calculated for different numbers of holes layers (N) for the fiber with Kagome lattice and 40 mol% of GeO_2 doping, Φ_c = 2.5 μm, Λ = 3.8 μm, and Φ_h = 0.25 μm (a) and 20 mol% of GeO_2 doping, Φ_c = 3.0 μm, Λ = 4.0 μm and Φ_h = 0.25 μm (b).

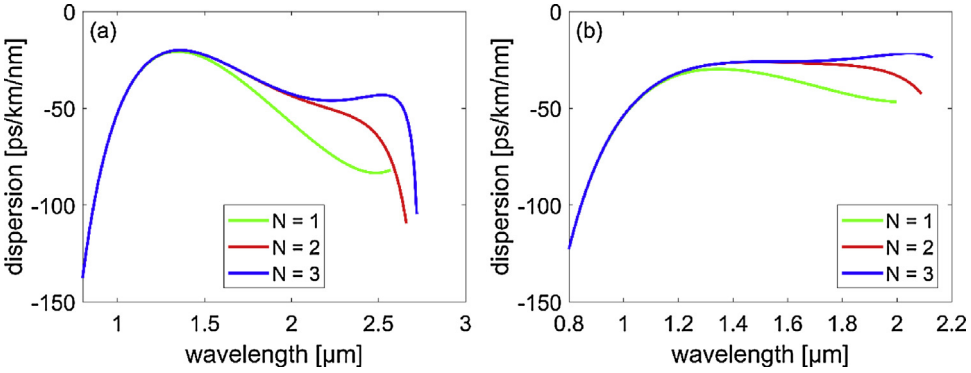

Fig. 7. Chromatic dispersion calculated for different numbers of holes layers (N) for the fiber with combined hexagonal and Kagome lattice for 40 mol% of GeO_2 doping, Φ_c = 2.5 μm, Λ = 3.3 μm, and Φ_h = 0.25 μm (a) and 20 mol% of GeO_2 doping, Φ_c = 3.0 μm, Λ = 3.6 μm and Φ_h = 0.20 μm (b).

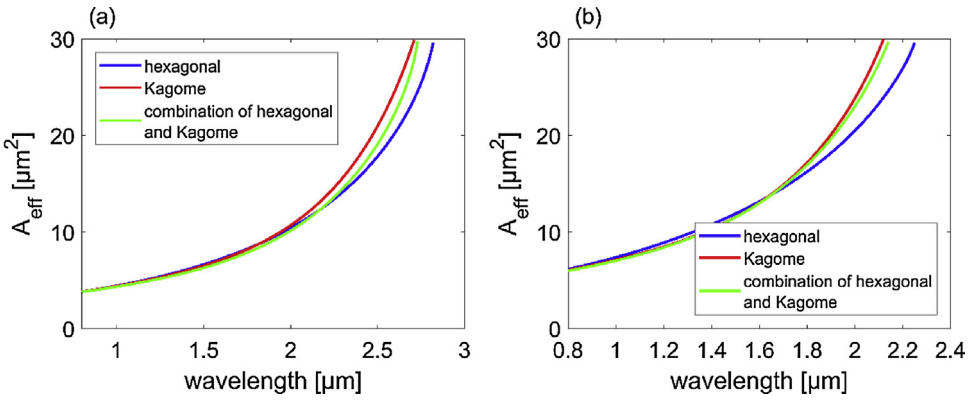

Fig. 8. Spectral dependence of the effective mode area calculated for optimal geometries of the examined fibers of the hexagonal, Kagome and combined lattices for 40 mol% of GeO_2 doping (a) and 20 mol% of GeO_2 doping (b).

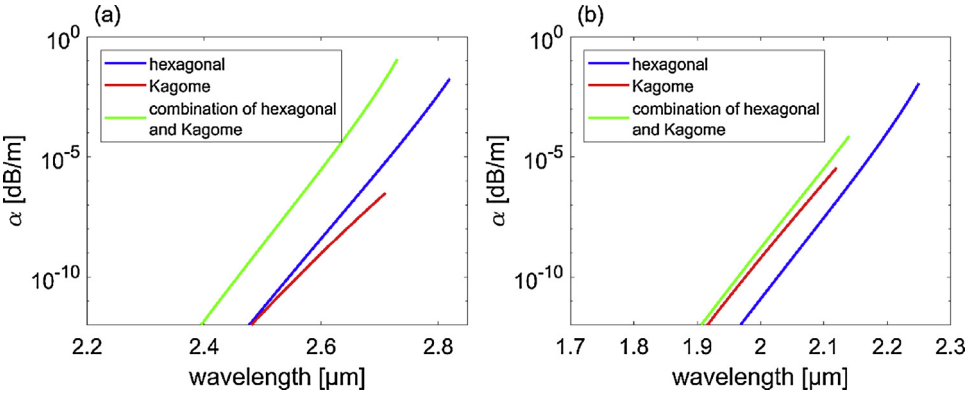

Fig. 9. Spectral dependence of the confinement loss calculated for optimal geometries of the examined fibers of the hexagonal, Kagome and combined lattices for 40 mol% of GeO_2 doping (a) and 20 mol% of GeO_2 doping (b).

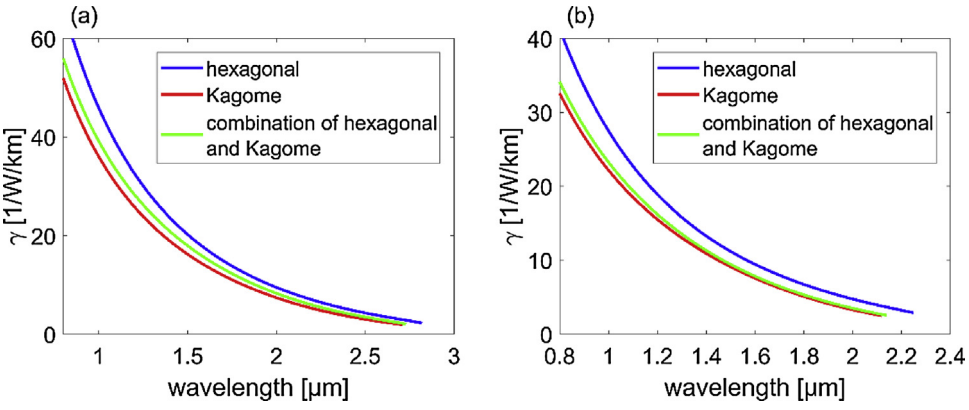

Fig. 10. Spectral dependence of the nonlinear coefficient γ for optimal geometries of the examined fibers of the hexagonal, Kagome and combined lattices for 40 mol% of GeO_2 doping (a) and 20 mol% of GeO_2 doping (b).

Table 1
Optimal fiber parameters (doping level, core diameters Φ_c, lattice constants Λ and holes diameters Φ_h) assuring the broadest normal dispersion range, up to λ_{max} wavelength under the condition of $A_{eff} \leq 30\,\mu m^2$.

core doping core diameter and N		hexagonal lattice	Kagome lattice	combination of hexagonal and Kagome lattice
40 mol%	$\Lambda\,[\mu m]$	2.8	3.8	3.3
$\Phi_c = 2.5\,\mu m$	$\Phi_h\,[\mu m]$	0.40	0.25	0.25
$N = 3$	λ_{max} [μm]	2.81	2.70	2.72
20 mol%	$\Lambda\,[\mu m]$	3.2	4.0	3.6
$\Phi_c = 3\,\mu m$	$\Phi_h\,[\mu m]$	0.40	0.25	0.20
$N = 3$	λ_{max} [μm]	2.25	2.11	2.13

In Table 1 we gathered the optimal parameters of the fibers with different symmetries assuring the greatest normal dispersion range and $A_{eff} \leq 30\,\mu m^2$. Our analysis shows that the largest normal dispersion range up to 2.81 μm is obtained for the fiber of hexagonal symmetry with 40 mol% of GeO_2 doping in the core and the following geometrical parameters: core diameter $\Phi_c = 2.5$ μm, lattice constant $\Lambda = 2.8$ μm, holes diameter $\Phi_h = 0.40$ μm, number of hole layers $N = 3$. It should be underlined that fabrication of such a fiber is absolutely possible with the use of stack and draw technology.

4. Conclusions

Our numerical analysis shows that increasing the GeO_2 doping level in the core of the step index fibers is beneficial for extending

the normal dispersion range. In particular, we have demonstrated that for the step-index fiber with 40 mol% of GeO_2 doping in the core and the core diameter of $\Phi_c = 2.5$ μm, the normal dispersion range extends up to 2.75 μm. Further increase in the normal dispersion range with the limited effective mode area can be enforced by addition of the microstructured cladding surrounding the core. Three cladding symmetries, i.e., hexagonal, Kagome and the combination of both, have been studied in this context. The greatest increase in the normal dispersion range up to 2.81 μm, while keeping $A_{eff} \leq 30\ \mu m^2$, has been obtained for the fiber with hexagonal symmetry. The calculated parameters, such as the core diameter $\Phi_c = 2.5$ μm, lattice constant $\Lambda = 2.8$ μm, holes diameter $\Phi_h = 0.40$ μm, number of hole layers $N = 3$, make the fabrication of such a fiber perfectly possible using the stack and draw technology. For the Kagome lattice and the combined lattice, a smaller increase in the normal dispersion range was observed. Further studies will include solving the nonlinear Schrödinger equation to determine the optimal pumping condition for designed fibers, particularly in terms of a central wavelength.

Acknowledgements

The work is supported by the National Science Centre, Poland, within the project no. 2014/13/D/ST7/02090 financed in the framework of SONATA 7 Program.

References

[1] J.K. Ranka, R.S. Windeler, A.J. Stentz, Visible continuum generation in air-silica microstructure optical fibers with anomalous dispersion at 800 nm, Opt. Lett. 25 (1) (2000) 25–27.
[2] I. Hartl, C. Chudoba, X.D. Li, R.K. Ghanta, T.H. Ko, J.G. Fujimoto, J.K. Ranka, R.S. Windeler, Ultrahigh-resolution optical coherence tomography using continuum generation in an air-silica microstructure optical fiber, Opt. Lett. 26 (9) (2001) 608–610.
[3] T. Lindfors, P. Stoller, V. Sandoghdar, Detection and spectroscopy of gold nanoparticles using supercontinuum white light confocal microscopy, Phys. Rev. Lett. vol. 93 (3) (2004), p. 037401.
[4] T.A. Birks, W.J. Wadsworth, P.S. Russell, Supercontinuum generation in tapered fibers, Opt. Lett. 25 (19) (2000) 1415–1417.
[5] J. Dudley, G. Genty, S. Coen, Supercontinuum generation in photonic crystal fiber, Rev. Mod. Phys. 78 (4) (2006) 1135–1184.
[6] M. Heidt, A. Hartung, G. Bosman, P. Krok, E. Rochwer, E. Schwoerer, H. Bartlelt, Coherent octave spanning near-infrared and visible supercontinuum generation in all-normal dispersion photonic crystal fibers, Opt. Express 19 (4) (2011) 3775–3787.
[7] M. Heidt, Pulse preserving flat-top supercontinuum generation in all-normal dispersion photonic crystal fibers, J. Opt. Soc. Am. B Opt. Phys. 27 (3) (2010) 550–559.
[8] M. Klimczak, G. Soboń, R. Kasztelanic, K. Abramski, R. Buczyński, Direct comparison of shot-to-shot noise performance of all normal dispersion and anomalous dispersion supercontinuum pumped with sub-picosecond pulse fiber-based laser, Sci. Rep. 6 (1928) 2016.
[9] C.C. Wang, H.M. Wang, J. Wu, Heavily germanium-doped silica fiber with a flat normal dispersion profile, IEEE Photonics J. 7 (2) (2015) 7101110.
[10] S.K. Chatterjee, S.N. Khan, P. Chaudhuri, Designing a two-octave spanning flat-top supercontinuum source by control of nonlinear dynamics through multi-order dispersion engineering in binary multi-clad microstructured fiber, J. Opt. Soc. Am. B 32 (7) (2015) 1499–1509.
[11] T. Martynkien, D. Pysz, R. Stępień, R.R. Buczyński, All-solid microstructured fiber with flat normal chromatic dispersion, Opt. Lett. 39 (8) (2014) 2342–2345.
[12] M. Klimczak, B. Siwicki, P. Skibiński, D. Pysz, R. Stępień, A. Heidt, C. Radzewicz, R. Buczyński, Coherent supercontinuum generation up to 2.3 μm in all-solid soft-glass photonic crystal fibers with flat all-normal dispersion, Opt. Express 22 (15) (2014) 18824–18832.
[13] S. Kedenburg, T. Steinle, F. Mörz, A. Steinmann, H. Giessen, High-power mid-infrared high repetition-rate supercontinuum source based on a chalcogenide step-index fibe, Opt. Lett. 40 (11) (2015) 2668–2671.
[14] L. Liu, T. Cheng, K. Nagasaka, H. Tong, G. Qin, T. Suzuki, Y. Ohishi, Coherent mid-infrared supercontinuum generation in all-solid chalcogenide microstructured fibers with all-normal dispersion, Opt. Lett. 41 (2) (2016) 392–395.
[15] C. Strutynski, P. Froidevaux, F. Désévédavy, J. Jules, G. Gadret, A. Bendahmane, K. Tarnowski, B. Kibler, F. Smektala, Tailoring supercontinuum generation beyond 2 μm in step-index tellurite fibers, Opt. Lett. 42 (2) (2017) 247–250.
[16] T. Hori, J. Takayanagi, N. Nishizawa, T. Goto, Flatly broadened, wideband and low noise supercontinuum generation in highly nonlinear hybrid fiber, Opt. Express 12 (2) (2004) 317–324.
[17] C. Xia, M. Kumar, M.Y. Cheng, O.P. Kulkarni, M.N. Islam, A. Galvanauskas, F.L. Terry, M.J. Freeman, D.A. Nolan, W.A. Wood, Supercontinuum generation in silica fibers by amplified nanosecond laser diode pulses, IEEE J. Sel. Top. Quantum Electron. 13 (3) (2007) 789–797.
[18] K. Tarnowski, W. Urbańczyk, All-normal dispersion hole-assisted silica fibers for generation of supercontinuum reaching midinfrared, IEEE Photonics J. 8 (1) (2016) 7100311.
[19] K. Tarnowski, T. Martynkien, P. Mergo, K. Poturaj, G. Soboń, W. Urbańczyk, Coherent supercontinuum generation up to 2.2 um in all-normal dispersion microstructured silica fiber, Opt. Express 22 (15) (2016) 30523–30536.
[20] K. Tarnowski, T. Martynkien, P. Mergo, K. Poturaj, A. Anuszkiewicz, P. Béjot, F. Billard, O. Faucher, B. Kibler, U. Urbanczyk, Polarized all-normal dispersion supercontinuum reaching 2.5 μm generated in a birefringent microstructured silica fiber, Opt. Express 25 (22) (2017) 27452–27463.
[21] I. Sukhoivanov, S. Iakushev, O. Shulika, E. Silvestre, M. Andres, Design of all-normal dispersion microstructured optical fiber on silica platform for generation of pulse-preserving supercontinuum under excitation at 1550 nm, J. Lightwave Technol. (99) (2017).
[22] R.B. Dyott, Elliptical Fiber Waveguides, Artech, 1995.
[23] H. Sunak, S. Bastien, Refractive index and material dispersion interpolation of doped silica in the 0. 6–1.8 μm wavelength region, IEEE Photonics 1 (6) (1989) 142–145.
[24] K. Nakajima, M. Ohashi, Dopant dependence of effective nonlinear refractive index in GeO_2- and F-doped core single-mode fibers, IEEE Photonics Techno. Lett. 14 (4) (2002) 492–494.
[25] J. Kobelke, K. Schuster, D. Litzkendorf, A. Schwuchow, J. Kirchhof, V. Tombelaine, H. Bartelt, P. Leproux, V. Couderc, A. Labruyere, R. Jamier, Highly germanium and lanthanum modified silica based glasses in microstructured optical fibers for non-linear applications, Opt. Mater. 32 (9) (2010) 1002–1006.